Article

Synthesis, Structure and Antimicrobial Activity of New Co(II) Complex with *bis*-Morpholino/Benzoimidazole-*s*-Triazine Ligand

Saied M. Soliman [1,*], Eman M. Fathalla [1], Mona M. Sharaf [2], Ayman El-Faham [1], Assem Barakat [3], Matti Haukka [4], Alexandra M. Z. Slawin [5], John Derek Woollins [5,6] and Morsy A. M. Abu-Youssef [1,*]

[1] Department of Chemistry, Faculty of Science, Alexandria University, P.O. Box 426, Ibrahimia, Alexandria 21321, Egypt; eman.nomeir@alexu.edu.eg (E.M.F.); ayman.elfaham@alexu.edu.eg (A.E.-F.)

[2] Protein Research Department, Genetic Engineering and Biotechnology Research Institute, City of Scientific Research and Technological Applications, Alexandria P.O. Box 21933, Egypt; sharafmona4@gmail.com

[3] Department of Chemistry, College of Science, King Saud University, P.O. Box 2455, Riyadh 11451, Saudi Arabia; ambarakat@ksu.edu.sa

[4] Department of Chemistry, University of Jyväskylä, P.O. Box 35, FI-40014 Jyväskylä, Finland; matti.o.haukka@jyu.fi

[5] School of Chemistry, University of St Andrews, St Andrews KY16 9ST, UK; amzs@st-andrews.ac.uk (A.M.Z.S.); jdw3@st-andrews.ac.uk (J.D.W.)

[6] Department of Chemistry, Khalifa University, Abu Dhabi P.O. Box 127788, United Arab Emirates

[*] Correspondence: saeed.soliman@alexu.edu.eg (S.M.S.); morsy5@alexu.edu.eg (M.A.M.A.-Y.)

Abstract: A new Co(II) perchlorate complex of the *bis*-morpholino/benzoimidazole-*s*-triazine ligand, 4,4′-(6-(1*H*-benzo[d]imidazol-1-yl)-1,3,5-triazine-2,4-diyl)dimorpholine (**BMBIT**), was synthesized and characterized. The structure of the new Co(II) complex was approved to be [Co(BMBIT)$_2$(H$_2$O)$_4$] (ClO$_4$)$_2$*H$_2$O using single-crystal X-ray diffraction. The Co(II) complex was found crystallized in the monoclinic crystal system and $P2_1/c$ space group. The unit cell parameters are a = 22.21971(11) Å, b = 8.86743(4) Å, c = 24.38673(12) Å and β = 113.4401(6)°. This heteroleptic complex has distorted octahedral coordination geometry with two monodenatate **BMBIT** ligand units via the benzoimidazole N-atom and four water molecules as monodentate ligands. The hydration water and perchlorate ions participated significantly in the supramolecular structure of the [Co(**BMBIT**)$_2$(H$_2$O)$_4$](ClO$_4$)$_2$*H$_2$O complex. Analysis of d$_{norm}$ map and a fingerprint plot indicated the importance of O···H, N···H, C···H, C···O, C···N and H···H contacts. Their percentages are 27.5, 7.9, 14.0, 0.9, 2.8 and 43.5%, respectively. The sensitivity of some harmful microbes towards the studied compounds was investigated. The Co(II) complex has good antifungal activity compared to the free **BMBIT** which has no antifungal activity. The Co(II) complex has good activity against *B. subtilis*, *S. aureus*, *P. vulgaris* and *E. coli* while the free **BMBIT** ligand has limited activity only towards *B. subtilis* and *P. vulgaris*. Hence, the [Co(**BMBIT**)$_2$(H$_2$O)$_4$](ClO$_4$)$_2$*H$_2$O complex has broad spectrum antimicrobial action compared to the free **BMBIT** ligand.

Keywords: Co(II); *bis*-morpholino/benzoimidazole-*s*-triazine; Hirshfeld; X-ray structure; antimicrobial

1. Introduction

Heterocyclic rings are the main constituent of many compounds in natural and synthetic drugs. Therefore, the scientific exploration of new heterocyclic molecular systems has attracted many chemists in the field of inorganic and organic chemistry [1–5]. In particular, *s*-triazine heterocycles are important nitrogen heterocyclic molecules. They are six-membered benzene rings incorporating three nitrogen atoms and three carbons. This interesting and exciting *s*-triazine scaffold has shown many possible applications which have been reviewed recently [6–9]. In the medical field, many representative examples incorporating the symmetrical rigid structure of the *s*-triazine scaffold have been

synthesized, characterized and explored in pharmacological applications against different targets [10]. These applications include the use of *s*-triazine derivatives as anticancer [11,12], antimicrobial [13], antiviral [14], and antiprotozoal agents [15].

From this point of view, the incorporation of the benzimidazole scaffold as a very important pharmacophore with *s*-triazine in one molecule was explored and the results indicated the enhancement of biological activity in the case of the organic hybrid. Singa et al. reported a series of *s*-triazine molecules clubbed with benzimidazole scaffolds which were assessed against different cancer cells, including breast cancer, colon cancer, melanoma, leukemia, ovarian cancer, non-small cell lung cancer and central nervous system tumours. They exhibited a median growth inhibitory (GI_{50}) in the range of 1.91–2.72 µM. The DNA intercalation and dihydrofolate reductase inhibition was optimized by the same research group [16,17]. Kumar et al. demonstrated the anticancer reactivity and SAR for a set of compounds based on *s*-triazine with different heterocycles, such as benzimidazole and benzothiazole scaffolds. Interestingly, a noticeable enhancement in the cytotoxic activity was found due to benzimidazole moity and the IC_{50} was found to be only 4.8 µM, indicating strong potency against breast cancer cell line MCF-7 [18]. Another example was presented by Singa et al. in the form of *s*-triazine-benzimidazole derivatives. They constructed and tested *s*-triazine-benzimidazole derivatives for antiproliferative potential against a panel of cancer cell lines and for investigating the bovine serum albumin interaction, which exhibited the highest inhibiting potency [19].

s-Triazines as ligands were studied extensively in coordination chemistry [9]. Refaat et al. designed a pincer ligand-based *s*-triazine with two arms of pyrazole scaffolds metalled with cobalt. They explored the cytotoxicity activity against two cancer cells including breast (MCF-7) and lung (A549). The results revealed that the Co(II)-pincer complexes exhibited good anticancer reactivity against the two cancer cell lines with IC_{50} = 15.31 ± 1.76 µM and 25.01 ± 2.29 for (MCF-7) and lung (A549), respectively [20]. Another example is the *s*-triazine-bridged calixarene explored in coordination chemistry with metal ions such as Co^{3+}, Fe^{3+} and Cr^{3+} [21]. The same research group explored metal complex-based tetraoxocalix[2], arene[2] and triazine for thermal and magnetic properties [22]. Several examples were reported and showed the utilization of *s*-triazine ligands for complexation with cobalt. The *s*-triazine ligands and cobalt were also explored as a catalyst for chemical synthesis transformation or medical uses [23–35], but the cobalt metal complex-based *s*-triazine clubbed with the benzimidazole scaffold has not yet been explored.

Recently, we reported the X-ray structure studies of some metal(II) complexes with hydrazino-*s*-triazine ligands 2,4-*bis*(morpholin-4-yl)-6-[(*E*)-2-[1-(pyridin-2-yl) ethylidene] hydrazin-1-yl]-1,3,5-triazine (**DMPT**) [36,37] and (*E*)-2,4-di(piperidin-1-yl)-6-(2-(1-(pyridin-2-yl)ethylidene)hydrazinyl)-1,3,5-triazine (**DPPT**) [38]. Their biological activities as antimicrobial agents against different harmful microbes were presented and compared with the corresponding free ligands. It was observed that the metal complexes of **DMPT** and **DPPT** have promising antibacterial and antifungal activities compared to the free **DMPT** and **DPPT** molecules. In extension to our work with the hydrazino-*s*-triazine ligands and based on the interesting bioactivity of both *s*-triazine and benzomidazole scaffolds, we designed a novel *s*-triazine-benzimidazole organic hybrid as a starting ligand for the preparation of a new Co(II) complex. Herein, we report the synthesis and antimicrobial evaluations of a new Co(II) complex with the hydrazino-*s*-triazine ligand, 4′-(6-(1H-benzo[d]imidazol-1-yl)-1,3,5-triazine-2,4-diyl) dimorpholine, shown in Figure 1. The molecular and supramolecular architectures of the studied complex were investigated using single-crystal X-ray diffraction analysis. Antimicrobial evaluations of both compounds are presented.
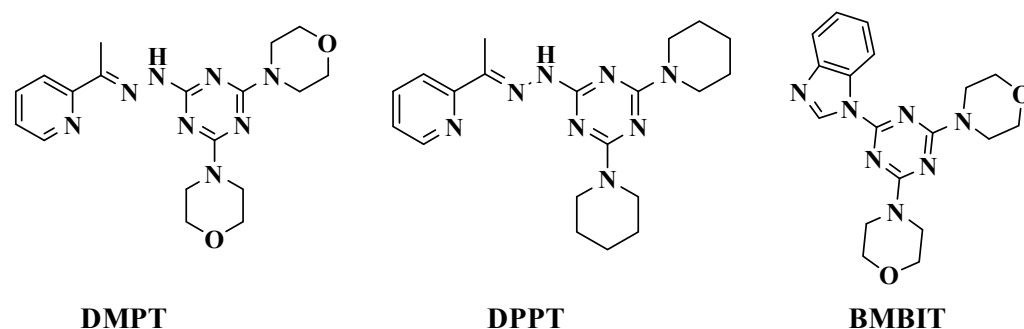
Figure 1. Structure of 2,4-*bis*(morpholin-4-yl)-6-[(*E*)-2-[1-(pyridin-2-yl)ethylidene] hydrazin-1-yl]-1,3,5-triazine, (**DMPT**) [36,37], (*E*)-2,4-di(piperidin-1-yl)-6-(2-(1-(pyridin-2-yl)ethylidene)hydrazinyl)-1,3,5-triazine (**DPPT**) [38] and the new 4,4′-(6-(1H-benzo[d]imidazol-1-yl)-1,3,5-triazine-2,4-diyl) dimorpholine (**BMBIT**).

2. Results

2.1. Synthesis and Characterizations

The new *bis*-morpholino/benzoimidazole *s*-triazine (**BMBIT**) ligand was synthesized following the reported method by Matsuno et al. [39] as indicated in Scheme 1. Cyanuric chloride **1** was first reacted with benzoimidazole **2** in an acetone–water mixture (1:1) in presence of $NaHCO_3$ at 0 °C for two hours and crushed ice was added to obtain the dichlorobenzoimidazole *s*-triazine derivative **3** as a white solid in good yield and purity, as observed for its NMR spectra.
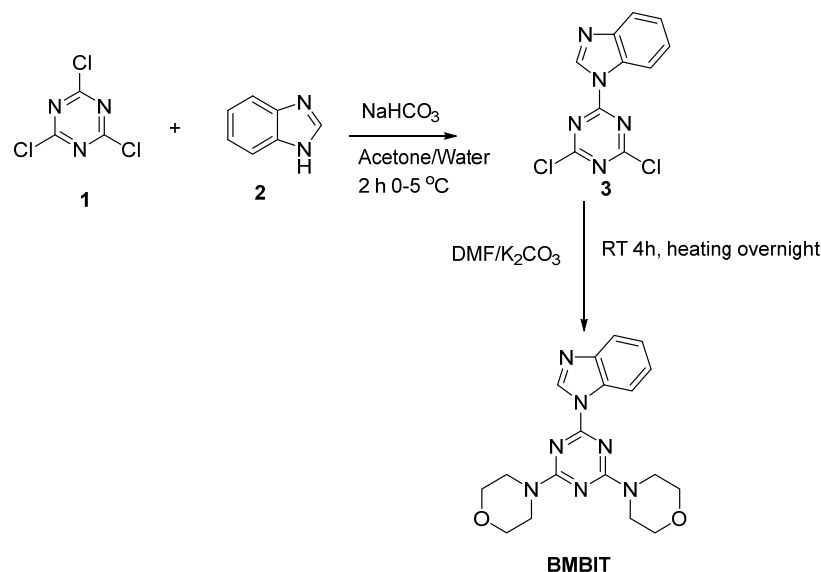
Scheme 1. Synthesis of the **BMBIT**.

The target *bis*-morpholino/benzoimidazole *s*-triazine (**BMBIT**) ligand was obtained from the reaction of **3** with two equivalents of morpholine in the presence of K_2CO_3 using dimethylformamide as the solvent under heating conditions [39] (Scheme 1) to obtain the target product, 4,4′-(6-(1H-benzo[d]imidazol-1-yl)-1,3,5-triazine-2,4-diyl)dimorpholine (**BMBIT**), in excellent yield and purity, which was used directly in the complexation process (Scheme 2). Following this, self-assembly of the ethanolic solutions of the *bis*-morpholino/benzoimidazole *s*-triazine (**BMBIT**) ligand and $Co(ClO_4)_2 \cdot 6H_2O$ was used to obtain the [Co(**BMBIT**)$_2$(H$_2$O)$_4$](ClO$_4$)$_2$*H$_2$O complex as a single-crystalline product (Scheme 2). The elemental analysis of the target complex confirmed the purity of the [Co(**BMBIT**)$_2$(H$_2$O)$_4$](ClO$_4$)$_2$*H$_2$O complex and its composition, which is further revealed by single-crystal X-ray structure analysis.
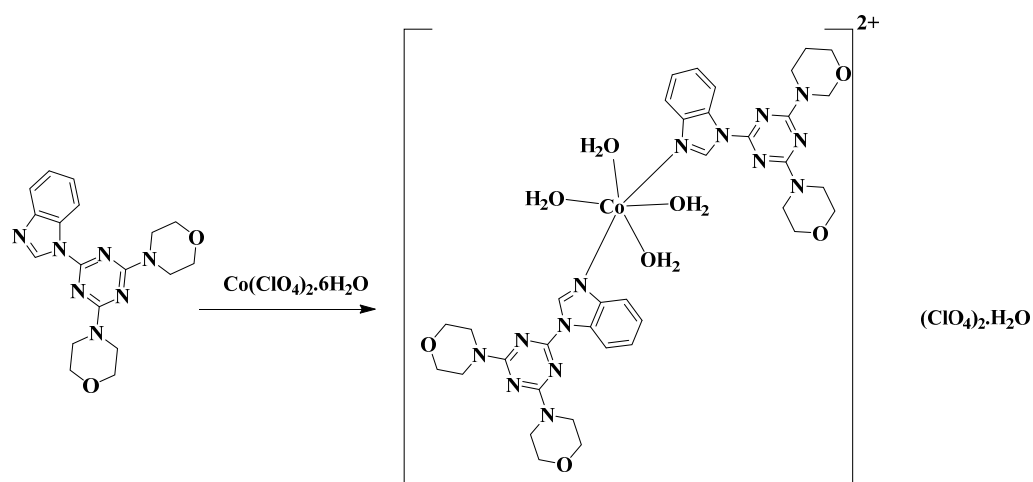
Scheme 2. Synthesis of the [Co(**BMBIT**)$_2$(H$_2$O)$_4$](ClO$_4$)$_2$*H$_2$O complex.

The structural aspects of the [Co(**BMBIT**)$_2$(H$_2$O)$_4$](ClO$_4$)$_2$*H$_2$O complex were found in accordance with the FTIR spectra which confirm the coordination of the Co(II) ion with the azomethine nitrogen and also confirmed the involvement of the perchlorate ion in the structure (Figures S1 and S2 in Supplementary Materials). The FTIR spectra of the **BMBIT** ligand showed the $\nu_{(C=N)}$ at 1600 and 1580 cm^{-1} and the $\nu_{(C=C)}$ mode at 1498 cm^{-1}. In the case of the [Co(**BMBIT**)$_2$(H$_2$O)$_4$](ClO$_4$)$_2$*H$_2$O complex, the $\nu_{(C=N)}$ mode was detected at lower wavenumbers of 1584 and 1575 cm^{-1}. On the other hand, the $\nu_{(C=C)}$ mode was detected almost at the same wavenumber as for the free ligand. The $\nu_{(C=C)}$ mode for the [Co(**BMBIT**)$_2$(H$_2$O)$_4$](ClO$_4$)$_2$*H$_2$O complex was detected at 1498 cm^{-1}. In addition, a broad splitted band at 1107 and 1073 cm^{-1} was assigned for the $\nu_{(Cl-O)}$ vibrations, confirming the presence of the perchlorate anion.

2.2. X-ray Structure Description

The X-ray single-crystal structure of the newly synthesized complex was confirmed to be [Co(**BMBIT**)$_2$(H$_2$O)$_4$](ClO$_4$)$_2$*H$_2$O. The crystal system of this complex is monoclinic, and the space group is *P2$_1$/c*. The unit cell parameters are *a* = 22.21971(11) Å, *b* = 8.86743(4) Å, *c* = 24.38673(12) Å and *β* = 113.4401(6)°. The asymmetric formula of this complex is one [Co(**BMBIT**)$_2$(H$_2$O)$_4$](ClO$_4$)$_2$*H$_2$O formula. In the unit cell there are four [Co(**BMBIT**)$_2$(H$_2$O)$_4$](ClO$_4$)$_2$*H$_2$O molecules where the unit cell volume is 4408.44(4) Å^3 and the crystal density is 1.631 Mg/m^3. Presentation of the coordination sphere of the [Co(**BMBIT**)$_2$(H$_2$O)$_4$](ClO$_4$)$_2$*H$_2$O complex is shown in Figure 2.

This heteroleptic complex has a hexa-coordinated Co(II) ion which is coordinated to six ligand groups where all are monodentate. The two N-donor ligand groups are coordinated with Co(II) via the N7 and N8 atoms of the benzoimidazole moiety, where both ligand units are trans to one another. The corresponding Co1-N7 and Co1-N8 distances are 2.1436(13) and 2.1267(13) Å, respectively, while the N7-Co1-N8 bond angle is 173.36(5)°, which is close to the ideal value of 180° for the perfect octahedron. On the other hand, four water molecules are found coordinated with the Co1 atom via O1, O2, O3 and O4 atoms. The corresponding Co-O distances are 2.0878(12), 2.1160(11), 2.0817(12) and 2.1831(12) Å, respectively. The angles between the cis Co-O bonds are in the range of 85.99(5)° to 95.65(5)°, while the two trans O3-Co1-O1 and O2-Co1-O4 angles are 173.42(5) and 176.91(5)°, respectively (Table 1). Hence, the coordination geometry of the [Co(**BMBIT**)$_2$(H$_2$O)$_4$](ClO$_4$)$_2$*H$_2$O complex is a distorted octahedron.
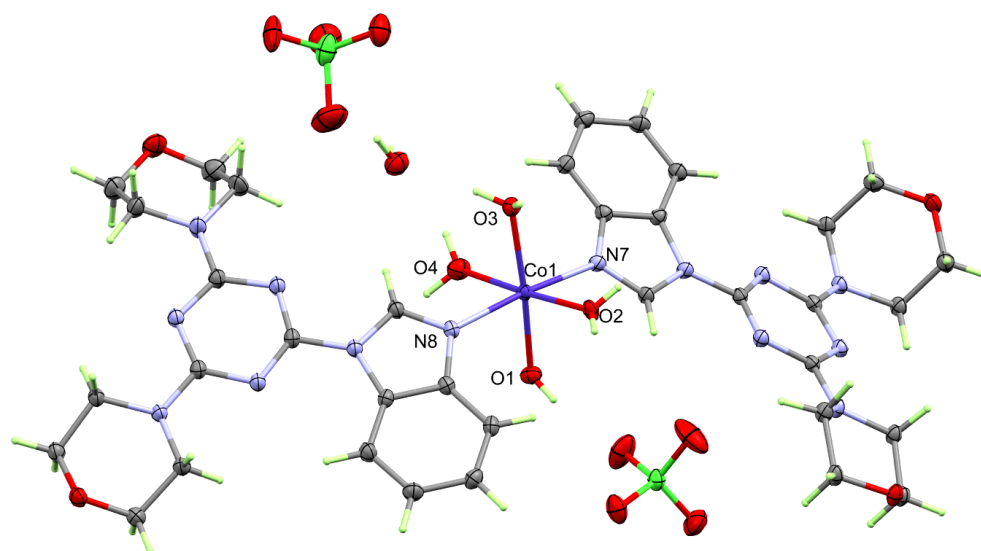
Figure 2. Structure of the coordination sphere of [Co(**BMBIT**)$_2$(H$_2$O)$_4$](ClO$_4$)$_2$*H$_2$O complex. One of the two perchlorate anions showed disorder and was omitted from this figure for better clarity.

Table 1. Bond distances and angles (Å and °) for the coordination environment of the [Co(**BMBIT**)$_2$(H$_2$O)$_4$](ClO$_4$)$_2$*H$_2$O complex.

Bond	Distance	Bond	Distance
Co(1)-O(3)	2.0817(12)	Co(1)-N(8)	2.1267(13)
Co(1)-O(1)	2.0878(12)	Co(1)-N(7)	2.1436(13)
Co(1)-O(2)	2.1160(11)	Co(1)-O(4)	2.1831(12)

Bonds	Angle	Bonds	Angle
O(3)-Co(1)-O(1)	173.42(5)	O(2)-Co(1)-N(7)	85.59(5)
O(3)-Co(1)-O(2)	90.88(5)	N(8)-Co(1)-N(7)	173.36(5)
O(1)-Co(1)-O(2)	95.65(5)	O(3)-Co(1)-O(4)	87.45(5)
O(3)-Co(1)-N(8)	93.49(5)	O(1)-Co(1)-O(4)	85.99(5)
O(1)-Co(1)-N(8)	86.56(5)	O(2)-Co(1)-O(4)	176.91(5)
O(2)-Co(1)-N(8)	96.50(5)	N(8)-Co(1)-O(4)	86.21(5)
O(3)-Co(1)-N(7)	92.77(5)	N(7)-Co(1)-O(4)	91.88(5)
O(1)-Co(1)-N(7)	86.96(5)		

It is worth noting that the structure of the [Co(**BMBIT**)$_2$(H$_2$O)$_4$](ClO$_4$)$_2$*H$_2$O complex contains one hydration water molecule and two perchlorate counter anions which are not involved in the coordination with the Co(II) ion but are significantly involved in the molecular packing of this complex (Figure 3A). The packing view of the [Co(**BMBIT**)$_2$(H$_2$O)$_4$](ClO$_4$)$_2$*H$_2$O complex along the crystallographic *ac*-direction is clearly seen from Figure 3B. In the [Co(**BMBIT**)$_2$(H$_2$O)$_4$](ClO$_4$)$_2$*H$_2$O complex, molecular packing is controlled by a number of O···H contacts. The coordinated and free water molecules are acting as H-bond donors while the perchlorate and the hydration water are H-bond acceptors. A list of the H-bond parameters is represented in Table 2. The majority of these intermolecular interactions are strong O-H···O hydrogen bonds, and the donor to acceptor distances are in the range of 2.7011(16) Å (O2-H2B···O6) to 3.082(3) Å (O4-H4A···O14). The respective hydrogen to acceptor distances are 1.91(3) and 2.18(4) Å.

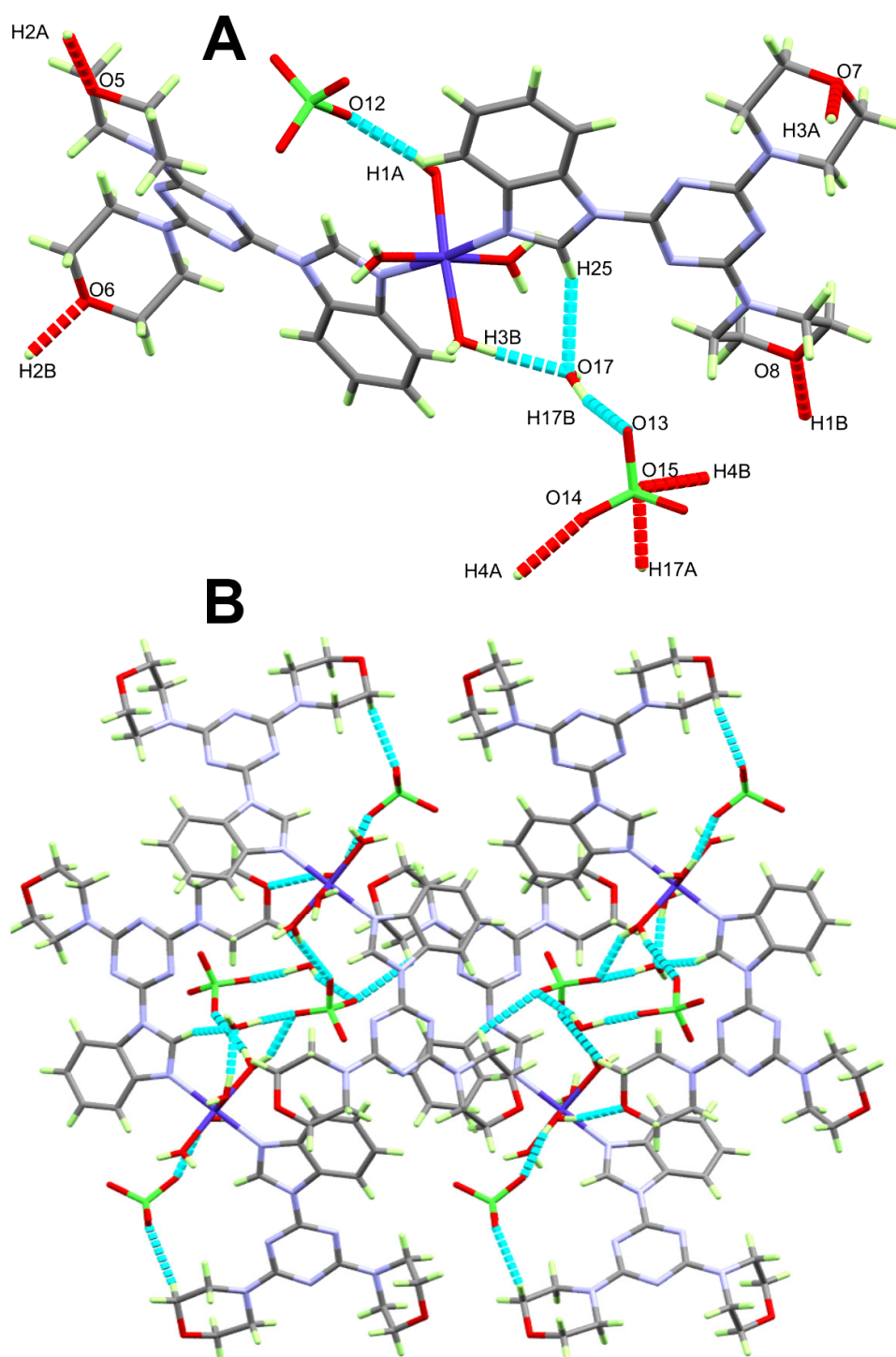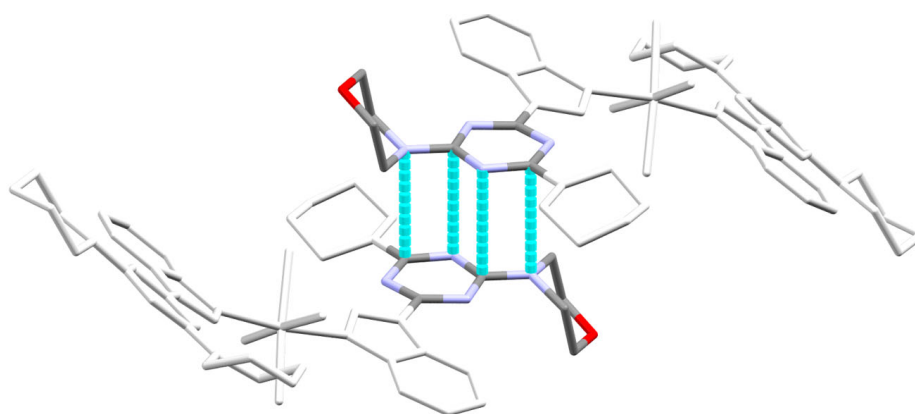**Figure 3.** Packing views of the $[Co(\textbf{BMBIT})_2(H_2O)_4](ClO_4)_2 \cdot H_2O$ complex.

The *s*-triazine ring from one complex molecule and the morpholine ring from another complex unit are found in close contact, whereas the C5⋯N3 and C6⋯N2 are the shortest contacts between the two ring systems (Figure 4). The respective contact distances are 3.247 and 3.222 Å.

Table 2. Hydrogen bond geometric parameters in the [Co(**BMBIT**)$_2$(H$_2$O)$_4$](ClO$_4$)$_2$*H$_2$O complex.

D-H . . . A	D-H	H···A	D···A	D-H···A
C7-H7A···O3 [#1]	0.98	2.4	3.292(6)	150.6
O(1)-H(1A)···O(12)	0.78(2)	1.98(2)	2.7418(19)	168(2)
O(1)-H(1B)···O(8) [#1]	0.85(3)	1.93(3)	2.7533(18)	165(3)
O(2)-H(2A)···O(5) [#2]	0.82(3)	2.06(3)	2.8337(16)	159(2)
O(2)-H(2B)···O(6) [#3]	0.79(3)	1.91(3)	2.7011(16)	174(3)
O(3)-H(3A)···O(7) [#4]	0.82(3)	1.92(3)	2.7209(17)	166(3)
O(3)-H(3B)···O(17)	0.86(3)	1.89(3)	2.7436(18)	174(3)
O(4)-H(4A)···O(14) [#5]	0.92(4)	2.18(4)	3.082(3)	168(3)
O(4)-H(4B)···O(15) [#1]	0.87(3)	2.01(3)	2.806(4)	153(3)
C(25)-H(25)···O(17)	0.95	2.43	3.286(2)	150
O(17)-H(17B)···O(13)	0.93	2.03	2.914(4)	157.4
O(17)-H(17A)···O(15) [#1]	0.94(4)	1.98(5)	2.797(5)	143(4)

[#1] $-x + 1, y + 1/2, -z + 1/2$; [#2] $-x + 2, y - 1/2, -z + 1/2$; [#3] $-x + 2, -y + 1, -z + 1$; [#4] $-x + 1, -y + 1, -z$; [#5] $x, y + 1, z$.

Figure 4. The shortest C···C contacts in the [Co(**BMBIT**)$_2$(H$_2$O)$_4$](ClO$_4$)$_2$*H$_2$O complex.

2.3. Analysis of Molecular Packing

The stability of the crystal structure is derived from many forces which keep the molecules arranged in a specific pattern to keep the crystal stable. The analysis of molecular packing with the help of Hirshfeld calculations provided all probable contacts in the crystal structure. The d$_{norm}$, curvedness and shape index surfaces for the [Co(**BMBIT**)$_2$(H$_2$O)$_4$](ClO$_4$)$_2$*H$_2$O complex are shown in Figure 5. The map of d$_{norm}$ gavea summary of all short contacts, which appear as red and white regions, indicating shorter and equal interaction distances than the vdWs radii sum of the interacting atoms. The longer contacts than the vdWs radii sum of the interacting atoms appeared as blue colored regions. Inspection of the d$_{norm}$ map indicated the importance of the O···H, N···H, C···H, C···O, C···N and H···H interactions in the molecular packing of the [Co(**BMBIT**)$_2$(H$_2$O)$_4$](ClO$_4$)$_2$*H$_2$O complex. These non-covalent interactions are labelled by letters **A** to **F**, respectively, for better clarity. A list of the shortest O···H, N···H, C···H, C···O, C···N and H···H interactions are given in Table 3.

The Hirshfeld analysis predicts all possible intermolecular contacts and their percentages in the crystal structure of the [Co(**BMBIT**)$_2$(H$_2$O)$_4$](ClO$_4$)$_2$*H$_2$O complex. Hence, it not only presents a qualitative summary of molecular packing but also quantitatively provides the percentages of these non-covalent interactions (Figure 6). The percentages of the O···H, N···H, C···H, C···O, C···N and H···H contacts are 27.5, 7.9, 14.0, 0.9, 2.8 and 43.5%, respectively. Hence, the intermolecular contacts involving hydrogen atom such as H···H, N···H, O···H and C···H are the most common in the crystal structure of the [Co(**BMBIT**)$_2$(H$_2$O)$_4$](ClO$_4$)$_2$*H$_2$O complex.
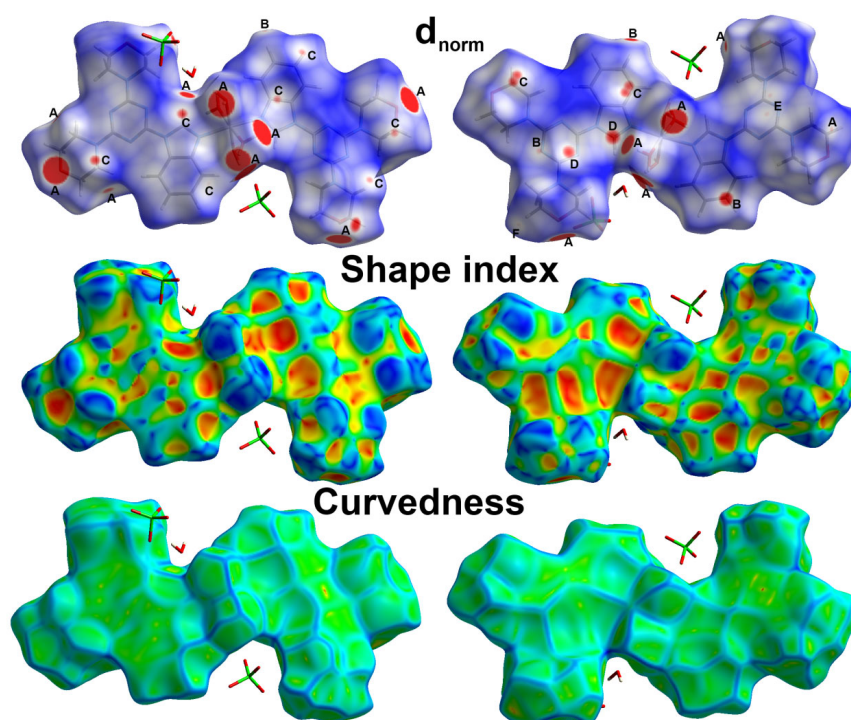
Figure 5. Hirshfeld surfaces for the [Co(**BMBIT**)$_2$(H$_2$O)$_4$](ClO$_4$)$_2$*H$_2$O complex.

Table 3. The short intermolecular interactions in the [Co(**BMBIT**)$_2$(H$_2$O)$_4$](ClO$_4$)$_2$*H$_2$O complex.

Contact	Distance	Contact	Distance
O5⋯H2A	1.902	C8⋯H2B	2.653
O7⋯H3A	1.760	C9⋯H2B	2.696
O6⋯H2B	1.722	C17⋯H8A	2.709
O15⋯H4B	1.904	C14⋯H4C	2.713
O16⋯H15	2.588	C14⋯H21	2.566
O11⋯H1C	2.557	C20⋯H3D	2.761
O10⋯H2C	2.445	C14⋯H21	2.566
O12⋯H1A	1.777	C35⋯H1B	2.665
O8⋯H1B	1.795	C25⋯H28A	2.651
O15⋯H17A	1.956	C19⋯H29A	2.683
O14⋯H4A	2.116	C20⋯H29A	2.680
O14⋯H35A	2.448	C29⋯H3A	2.647
O15⋯H17B	2.481	C30⋯H3A	2.711
O13⋯H17B	1.985	C2⋯H2A	2.768
O13⋯H28B	2.574	C6⋯N2	3.222
O12⋯H7A	2.560	C5⋯N3	3.247
O13⋯H28B	2.574	C25⋯O14	3.040
N12⋯H15	2.595	C32⋯O16	3.079
H7B⋯H34B	2.175		

The fingerprint plot shows a graphical representation of the distance between the surface and an atom inside the surface (d_i) against the distance between the surface and an atom outside the surface (d_i), which not only provides a quantitative summary for all possible intermolecular contacts (Figure 6) but also reveal their importance (Figure 7). It is clear that the decomposed fingerprint plots of the O⋯H, N⋯H, C⋯H, C⋯O, C⋯N and H⋯H contacts appear as sharp spikes. This pattern for the fingerprint plots is considered as strong evidence of a strong interaction occurring at short contact distances between the atoms.
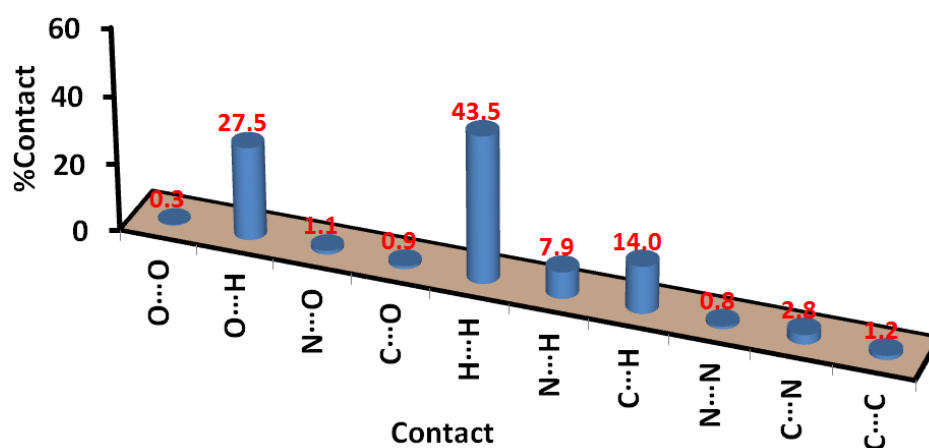
Figure 6. Intermolecular interactions in the [Co(**BMBIT**)$_2$(H$_2$O)$_4$](ClO$_4$)$_2$*H$_2$O complex.
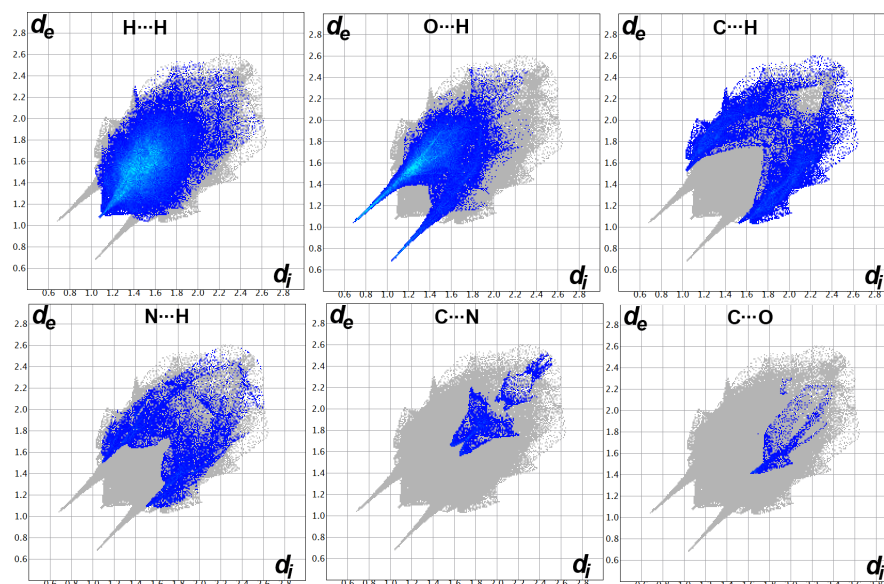
Figure 7. Fingerprint plots for the relevant contacts in the [Co(**BMBIT**)$_2$(H$_2$O)$_4$](ClO$_4$)$_2$*H$_2$O complex.

The different contacts that occurred at short distances are presented in Table 3. Interestingly, the Hirshfeld analysis detected the presence of anion-π stacking interactions as revealed by the presence of short C25···O14 (3.040 Å) and C32···O16 (3.079 Å), which occur between the perchlorate O-atom with the aromatic π-system of the benzoimidazole and s-triazine rings, respectively. The O6···H2B (1.722 Å), N12···H15 (2.595 Å), H7B···H34B (2.175 Å), C14···H21 (2.566 Å), C6···N2 (3.222 Å) and C25···O14 (3.040 Å) are the shortest non-covalent contacts in the crystal structure of the [Co(**BMBIT**)$_2$(H$_2$O)$_4$](ClO$_4$)$_2$*H$_2$O complex.

2.4. Antimicrobial Assay

The sensitivity of selected bacteria as *Staphylococcus aureus* and *Bacillus subtilis* (gram-positive), *Escherichia coli*, *Proteus vulgaris* (gram-negative) and fungi such as *Aspergillus fumigatus* and *Candida albicans* towards the free ligand **BMBIT** and [Co(**BMBIT**)$_2$(H$_2$O)$_4$](ClO$_4$)$_2$*H$_2$O complex were examined. Recently, the antimicrobial activity of the free ligands **DMPT** and **DPPT** were compared with their metal (II) complexes [36–38]. It was found that the majority of the studied metal (II) complexes have better antimicrobial activities than the free ligands [36–38]. In accordance with our previous studies, it was observed that the free ligand **BMBIT** has no effect on both fungal species *Aspergillus fumigatus* and *Candida albicans*. In contrast, the [Co(**BMBIT**)$_2$(H$_2$O)$_4$](ClO$_4$)$_2$*H$_2$O complex has good activity against both microbes. The inhibition zone diameters are 13 and 15 mm, respectively, while

the MIC values are 312 and 156 μg/mL, respectively. The results are relatively close to the antifungal agent Ketoconazole (Table 4).

Table 4. Antimicrobial activities of **BMBIT** and the [Co(**BMBIT**)$_2$(H$_2$O)$_4$](ClO$_4$)$_2$*H$_2$O complex [a].

Microorganism	BMBIT	[Co(BMBIT)$_2$(H$_2$O)$_4$](ClO$_4$)$_2$*H$_2$O	Control
A. fumigatus	NA [b] (ND) [c]	13(312)	17(156) [d]
C. albicans	NA [b] (ND) [c]	15(156)	20(312) [d]
S. aureus	NA [b] (ND) [c]	16(156)	24(9.7) [e]
B. subtilis	13 (312)	13(312)	26(4.8) [e]
E. coli	NA [b] (ND) [c]	15(156) [c]	30(4.8) [e]
P. vulgaris	13 (ND) [c]	17(78) [c]	25(4.8) [e]

[a] Inhibition zone diameter; mm (MIC; μg/mL) [b] NA: no activity; [c] ND: not determined; [d] Ketoconazole and [e] *Gentamycin.*

The free ligand showed some sensitivity towards the studied gram-positive and gram-negative bacteria. The free **BMBIT** ligand and the [Co(**BMBIT**)$_2$(H$_2$O)$_4$](ClO$_4$)$_2$*H$_2$O complex are active against the gram-positive bacteria *B. subtilis* and the gram-negative bacteria *P. vulgaris*. The inhibition zone diameters are 13 and 17 mm for the [Co(**BMBIT**)$_2$(H$_2$O)$_4$] (ClO$_4$)$_2$*H$_2$O complex and 13 mm for **BMBIT** against both microbes. It is clear that both compounds showed the same sensitivity against *B. subtilis* as both gave the same inhibition zone diameters and the same MIC value (312 μg/mL). For the gram-negative bacteria *P. vulgaris*, the [Co(**BMBIT**)$_2$(H$_2$O)$_4$](ClO$_4$)$_2$*H$_2$O complex has better activity compared to the free ligand. The MIC value for the Co(II) complex is only 78 μg/mL. In addition, the free **BMBIT** ligand is not active against both *S. aureus* and *E. coli*. In contrast, the [Co(**BMBIT**)$_2$(H$_2$O)$_4$](ClO$_4$)$_2$*H$_2$O complex showed inhibitions towards these microbes, with zone sizes of 16 and 15 mm, respectively. The respective MIC values are 156 μg/mL for both microbes. Hence, the [Co(**BMBIT**)$_2$(H$_2$O)$_4$](ClO$_4$)$_2$*H$_2$O complex has better antibacterial activity against all microbes than **BMBIT**. The antibacterial activity of the [Co(**BMBIT**)$_2$(H$_2$O)$_4$](ClO$_4$)$_2$*H$_2$O complex could be described as moderate with respect to the antibacterial agent *Gentamycin.* In comparison with the studied metal (II) complexes of the **DMPT** and **DPPT** ligands [36–38], the [Co(**BMBIT**)$_2$(H$_2$O)$_4$](ClO$_4$)$_2$*H$_2$O complex has more or less antibacterial activities. On the other hand, the [Co(**BMBIT**)$_2$(H$_2$O)$_4$](ClO$_4$)$_2$*H$_2$O complex has better antifungal activity against *Aspergillus fumigatus* and *Candida albicans* compared with the other metal (II) complexes. As a result, the [Co(**BMBIT**)$_2$(H$_2$O)$_4$](ClO$_4$)$_2$*H$_2$O complex is a broad-spectrum antimicrobial agent against the studied microbes. The interesting antimicrobial activity of the [Co(**BMBIT**)$_2$(H$_2$O)$_4$](ClO$_4$)$_2$*H$_2$O complex compared to the free ligand **BMBIT** could be explained in terms of its ability to prevent the microbes from protein production, leading to the death of the treated microbes [40].

3. Materials and Methods

3.1. Physical Measurements

All chemicals were bought from their commercial sources and used without additional purifications (see Supplementary Materials).

3.2. Synthesis of 4,4′-(6-(1H-benzo[d]imidazol-1-yl)-1,3,5-triazine-2,4-diyl)dimorpholine (BMBIT) Ligand [39]

First, dichlorobenzoimidazole **3** was synthesized as follows: benzimidazole (0.1 mole, 11.8 g) was dissolved in acetone (15 mL) and added to a solution of cyanuric chloride (0.1 mole, 18.4 g) in acetone (100 mL) at 0–5 °C, and sodium bicarbonate solution (0.12 mole in 100 mL water) was added over a period of 10 min to adjust the pH of the reaction mixture. The reaction mixture was continued stirring for 2 h at 0–5 °C, crushed ice was added and the solid obtained was filtered and dried. The product was recrystallized from ethanol and the pure product **3** was obtained as an off-white precipitate with an 88% yield, mp 118–120 °C.

^{1}H-NMR (400 MHz, DMSO-d_6, ppm): δ 7.39–7.45 (m, 2H, Ar-H), 7.76 (d, 1H, *J* = 7.6 Hz, Ar-H), 8.44 (d, 1H, *J* = 8.0 Hz, Ar-H), 9.16 (s, 1H, CH, Ar-H); ^{13}C-NMR (100 MHz, DMSO-d_6, ppm): δ 116.2, 119.8, 125.3, 131.1, 142.7, 143.6, 161.8, 163.4.

Compound **3** was reacted with morpholine to obtain the target product as follows: 2-(benzimidazol-1-yl)-4,6,-dichloro-*s*-triazine **3** (10 mmol) was stirred with morpholine (20 mmol) in 10 mL DMF in the presence of K_2CO_3 (22 mmol) at room temperature for 4 h and then heated at 80 °C overnight. The reaction mixture was poured into an ice-water mixture and the product was filtered, washed with ethanol and dried, to afford the target product **BMBIT** as a white solid with a 91% yield, mp. 223–225 °C (Lit. [39], yield 98%, mp.222–224 °C). Anal. Calc. $C_{18}H_{21}N_7O_2$: C, 58.84; H, 5.76; N, 26.69%. Found: C, 58.65; H, 5.64; N, 26.52%. IR (KBr, cm^{-1}): 3126 ν(C–H), 3058 ν(C–H), 2994 ν(C–H), 2903 ν(C–H), 1600 ν(C=N), 1580 ν(C=N), 1498 ν(C=C).

3.3. Synthesis of [Co(BMBIT)$_2$(H$_2$O)$_4$](ClO$_4$)$_2$*H$_2$O Complex

$Co(ClO_4)_2 \cdot 6H_2O$ (47.6 mg, 0.2 mmol) in 7 mL ethanol was mixed with an 8 mL ethanolic solution of organic ligand **BMBIT** (145.3 mg, 0.4 mmol). The resulting brown solution was allowed to evaporate slowly and crystallize at room temperature. After 1 week, reddish-brown crystals of [Co(**BMBIT**)$_2$(H$_2$O)$_4$](ClO$_4$)$_2$*H$_2$O complex were collected by filtration.

[Co(**BMBIT**)$_2$(H$_2$O)$_4$](ClO$_4$)$_2$*H$_2$O complex: Anal. Calc. $C_{36}H_{52}Cl_2CoN_{14}O_{17}$: C, 39.93; H, 4.84; N, 18.11; Co, 5.44%. Found: C, 39.70; H, 4.78; N, 17.98; Co, 5.37%. IR (KBr, cm^{-1}): 3113 ν(C–H), 3000 ν(C–H), 2969 ν (C–H), 2912 ν (C–H), 1584 ν(C=N), 1571 ν(C=N), 1497 ν(C=C), 1107 ν(Cl–O), 1073 ν(Cl–O).

3.4. Crystal Structure Determination

The crystal of the Co(II) complex was determined as described Method S1 in Supplementary Materials [41–44]. The crystallographic details are summarized in Table 5.

Table 5. Crystal data and refinement parameters.

CCDC	2266666
empirical formula	$C_{36}H_{52}Cl_2CoN_{14}O_{17}$
fw	1082.74
temp (K)	120(2)
λ(Å)	1.54184
cryst syst	Monoclinic
space group	P2$_\mathbf{1}$/c
a (Å)	22.21971(11)
b (Å)	8.86743(4)
c (Å)	24.38673(12)
β (deg)	113.4401(6)
V (Å^3)	4408.44(4)
Z	4
ρ_{calc} (Mg/m^3)	1.631
μ(Mo Kα) (mm^{-1})	4.967
No. reflns.	125499
Unique reflns.	9260
Completeness to θ = 67.684°	99.9%
GOOF (F^2)	1.036
R_{int}	0.0300
$R_1$$^{\text{a}}$ ($I \geq 2\sigma$)	0.0314
$wR_2$$^{\text{b}}$ ($I \geq 2\sigma$)	0.0841

$^{\text{a}}$ $R_1 = \Sigma||F_o| - |F_c||/\Sigma|F_o|$. $^{\text{b}}$ $wR_2 = \{\Sigma[w(F_o^2 - F_c^2)^2]/\Sigma[w(F_o^2)^2]\}^{1/2}$.

3.5. Hirshfeld Analysis

The Crystal Explorer Ver. 3.1 program [45] was used to perform this analysis.

3.6. Antimicrobial Assay

The antibacterial activity is declared in Supplementary Materials (Method S1) [46].

4. Conclusions

A new [Co(**BMBIT**)$_2$(H$_2$O)$_4$](ClO$_4$)$_2$*H$_2$O complex was synthesized by self-assembly of Co(II) perchlorate and 4,4′-(6-(1*H*-benzo[d]imidazol-1-yl)-1,3,5-triazine-2,4-diyl) dimorpholine (**BMBIT**) in ethanol. The three-dimensional structure and crystal-packing structure aspects of the [Co(BMBIT)$_2$(H$_2$O)$_4$](ClO$_4$)$_2$*H$_2$O complex were analyzed using single-crystal X-ray diffraction. The Co(II) is hexa-coordinated with a CoN$_2$O$_4$ coordination sphere. All ligand groups (**BMBIT** and H$_2$O) are monodentate and the cationic complex is monomeric with a distorted octahedral coordination geometry in the coordination sphere. The O···H, N···H, C···H, C···O, C···N and H···H intermolecular contacts contributed by 27.5, 7.9, 14.0, 0.9, 2.8 and 43.5%, respectively, in the supramolecular structure of the Co(II) complex. The [Co(**BMBIT**)$_2$(H$_2$O)$_4$](ClO$_4$)$_2$*H$_2$O complex has broad-spectrum antimicrobial action compared to the free **BMBIT** ligand. Mechanistic investigation of the biological activity will be considered in our future work.

References

1. Sun, H.; Chen, S.; Zhong, A.; Sun, R.; Jin, J.; Yang, J.; Liu, D.; Niu, J.; Lu, S. Tuning Photophysical Properties via Positional Isomerization of the Pyridine Ring in Donor–Acceptor-Structured Aggregation-Induced Emission Luminogens Based on Phenyl-methylene Pyridineacetonitrile Derivatives. *Molecules* **2023**, *28*, 3282. [CrossRef]
2. Ye, D.; Liu, L.; Peng, Q.; Qiu, J.; Gong, H.; Zhong, A.; Liu, S. Effect of Controlling Thiophene Rings on D-A Polymer Photocatalysts Accessed via Direct Arylation for Hydrogen Production. *Molecules* **2023**, *28*, 4507. [CrossRef] [PubMed]
3. Wang, K.; He, X.; Rong, C.; Zhong, A.; Liu, S.; Zhao, D. On the origin and nature of internal methyl rotation barriers: An information-theoretic approach study. *Theor. Chem. Acc.* **2022**, *141*, 68. [CrossRef]
4. Zhang, W.; Ye, G.; Liao, D.; Chen, X.; Lu, C.; Ejhieh, A.N.; Khan, M.S.; Liu, J.; Pan, Y.; Dai, Z. Recent Advances of Silver-Based Coordination Polymers on Antibacterial Applications. *Molecules* **2022**, *27*, 7166. [CrossRef] [PubMed]
5. Chen, J.; Zhang, Z.; Ma, J.; Nezamzadeh-Ejhieh, A.; Lu, C.; Pan, Y.; Liu, J.; Bai, Z. Current status and prospects of MOFs in controlled delivery of Pt anticancer drugs. *Dalton Trans.* **2023**, *52*, 6226–6238. [CrossRef] [PubMed]
6. Sharma, A.; Sheyi, R.; de la Torre, B.G.; El-Faham, A.; Albericio, F. *s*-Triazine: A Privileged Structure for Drug Discovery and Bioconjugation. *Molecules* **2021**, *26*, 864. [CrossRef]
7. Maliszewski, D.; Drozdowska, D. Recent Advances in the Biological Activity of *s*-Triazine Core Compounds. *Pharmaceuticals* **2022**, *15*, 221. [CrossRef]
8. Dai, Q.; Sun, Q.; Ouyang, X.; Liu, J.; Jin, L.; Liu, A.; He, B.; Fan, T.; Jiang, Y. Antitumor Activity of *s*-Triazine Derivatives: A Systematic Review. *Molecules* **2023**, *28*, 4278. [CrossRef]
9. Barakat, A.; El-Faham, A.; Haukka, M.; Al-Majid, A.M.; Soliman, S.M. *s*-Triazine pincer ligands: Synthesis of their metal complexes, coordination behavior, and applications. *Appl. Organomet. Chem.* **2021**, *35*, e6317. [CrossRef]

10. Majeed Ganai, A.; Khan Pathan, T.; Hampannavar, G.A.; Pawar, C.; Obakachi, V.A.; Kushwaha, B.; Deshwar Kushwaha, N.; Karpoormath, R. Recent Advances on the s-Triazine Scaffold with Emphasis on Synthesis, Structure-Activity and Pharmacological Aspects: A Concise Review. *ChemistrySelect* **2021**, *6*, 1616–1660. [CrossRef]

11. Shawish, I.; Barakat, A.; Aldalbahi, A.; Malebari, A.M.; Nafie, M.S.; Bekhit, A.A.; Albohy, A.; Khan, A.; Ul-Haq, Z.; Haukka, M.; et al. Synthesis and Antiproliferative Activity of a New Series of Mono- and Bis(dimethylpyrazolyl)-s-triazine Derivatives Targeting EGFR/PI3K/AKT/mTOR Signaling Cascades. *ACS Omega* **2022**, *7*, 24858–24870. [CrossRef]

12. Shawish, I.; Barakat, A.; Aldalbahi, A.; Alshaer, W.; Daoud, F.; Alqudah, D.A.; Al Zoubi, M.; Hatmal, M.M.; Nafie, M.S.; Haukka, M.; et al. Acetic Acid Mediated for One-Pot Synthesis of Novel Pyrazolyl s-Triazine Derivatives for the Targeted Therapy of Triple-Negative Breast Tumor Cells (MDA-MB-231) via EGFR/PI3K/AKT/mTOR Signaling Cascades. *Pharmaceutics* **2022**, *14*, 1558. [CrossRef] [PubMed]

13. Liu, H.; Long, S.; Rakesh, K.P.; Zha, G.F. Structure-activity relationships (SAR) of triazine derivatives: Promising antimicrobial agents. *Eur. J. Med. Chem.* **2020**, *185*, 111804. [CrossRef] [PubMed]

14. Krečmerová, M.; Dračínský, M.; Snoeck, R.; Balzarini, J.; Pomeisl, K.; Andrei, G. New prodrugs of two pyrimidine acyclic nucleoside phosphonates: Synthesis and antiviral activity. *Bioorg. Med. Chem.* **2017**, *25*, 4637–4648. [CrossRef] [PubMed]

15. Venkatraj, M.; Salado, I.G.; Heeres, J.; Joossens, J.; Lewi, P.J.; Caljon, G.; Maes, L.; Van der Veken, P.; Augustyns, K. Novel triazine dimers with potent antitrypanosomal activity. *Eur. J. Med. Chem.* **2018**, *143*, 306–319. [CrossRef]

16. Singla, P.; Luxami, V.; Paul, K. Synthesis, in Vitro Antitumor Activity, Dihydrofolate Reductase Inhibition, DNA Intercalation and Structure—Activity Relationship Studies of 1,3,5-Triazine Analogues. *Bioorg. Med. Chem. Lett.* **2016**, *26*, 518–523. [CrossRef]

17. Singla, P.; Luxami, V.; Paul, K. Triazine–Benzimidazole Hybrids: Anticancer Activity, DNA Interaction and Dihydrofolate Reductase Inhibitors. *Bioorg. Med. Chem.* **2015**, *23*, 1691–1700. [CrossRef]

18. Kumar, G.J.; Kumar, S.N.; Thummuri, D.; Adari, L.B.S.; Naidu, V.G.M.; Srinivas, K.; Rao, V.J. Synthesis and Characterization of New s-Triazine Bearing Benzimidazole and Benzothiazole Derivatives as Anticancer Agents. *Med. Chem. Res.* **2015**, *24*, 3991–4001. [CrossRef]

19. Singla, P.; Luxami, V.; Paul, K. Synthesis and in Vitro Evaluation of Novel Triazine Analogues as Anticancer Agents and Their Interaction Studies with Bovine Serum Albumin. *Eur. J. Med. Chem.* **2016**, *117*, 59–69. [CrossRef]

20. Refaat, H.M.; Alotaibi, A.A.M.; Dege, N.; El-Faham, A.; Soliman, S.M. Co (II) Complexes Based on the *Bis*-Pyrazol-s-Triazine Pincer Ligand: Synthesis, X-ray Structure Studies, and Cytotoxic Evaluation. *Crystals* **2022**, *12*, 741. [CrossRef]

21. Aouled, I.M.; Uysal, S. The synthesis and characterization of s-triazine bridged calixarene based a Schiff base: Investigation of its [MSalen/Salophen](M = Cr^{3+}, Fe^{3+} or Co^{3+}) capped complexes. *J. Mol. Struct.* **2022**, *1250*, 131872. [CrossRef]

22. Aouled, I.M.; Uysal, S. Investigation of thermal and magnetic properties of [MSalen/Saloph](M = Cr^{3+}, Fe^{3+} or Co^{3+}) capped dinuclear complexes of two novel tetraoxocalix[2]arene[2]triazine ligands. *J. Mol. Struct.* **2023**, *1280*, 135084. [CrossRef]

23. Cahiez, G.R.; Moyeux, A. Cobalt-catalyzed cross-coupling reactions. *Chem. Rev.* **2010**, *110*, 1435–1462. [CrossRef] [PubMed]

24. Hebrard, F.; Kalck, P. Cobalt-catalyzed hydroformylation of alkenes: Generation and recycling of the carbonyl species, and catalytic cycle. *Chem. Rev.* **2009**, *109*, 4272–4282. [CrossRef]

25. Junge, K.; Papa, V.; Beller, M. Cobalt–pincer complexes in catalysis. *Chem. Eur. J.* **2019**, *25*, 122–143. [CrossRef] [PubMed]

26. Pototschnig, G.; Maulide, N.; Schnürch, M. Direct functionalization of C−H bonds by iron, nickel, and cobalt catalysis. *Chem. Eur. J.* **2017**, *23*, 9206–9232. [CrossRef] [PubMed]

27. Yoshino, T.; Matsunaga, S. Cobalt-catalyzed $C(sp^3)$−H functionalization reactions. *Asian J. Org. Chem.* **2018**, *7*, 1193–1205. [CrossRef]

28. Tilly, D.; Dayaker, G.; Bachu, P. Cobalt mediated C–H bond functionalization: Emerging tools for organic synthesis. *Catal. Sci. Technol.* **2014**, *4*, 2756–2777. [CrossRef]

29. Asgharpour, Z.; Farzaneh, F.; Abbasi, A. Synthesis, characterization and immobilization of a new cobalt(ii) complex on modified magnetic nanoparticles as catalyst for epoxidation of alkenes and oxidation of activated alkanes. *RSC Adv.* **2016**, *6*, 95729–95739. [CrossRef]

30. Shao, D.; Shi, L.; Wei, H.Y.; Wang, X.Y. Field-induced single-ion magnet behavior in two new cobalt(II) coordination polymers with 2,4,6-tris(4-pyridyl)-1,3,5-triazine. *Inorganics* **2017**, *5*, 90. [CrossRef]

31. Osman, A.H. Synthesis and characterization of cobalt(II) and nickel(II) complexes of some Schiff bases derived from 3-hydrazino-6-methyl [1,2,4] triazin-5(4H)one. *Transit. Met. Chem.* **2006**, *31*, 35–41. [CrossRef]

32. Menati, S.; Rudbari, H.A.; Askari, B.; Farsani, M.R.; Jalilian, F.; Dini, G. Synthesis and characterization of insoluble cobalt(II), nickel(II), zinc(II) and palladium(II) Schiff base complexes: Heterogeneous catalysts for oxidation of sulfides with hydrogen peroxide. *Compets Rendus Chim.* **2016**, *19*, 347–356. [CrossRef]

33. Marandi, F.; Moeini, K.; Arkak, A.; Mardani, Z.; Krautscheid, H. Docking studies to evaluate the biological activities of the Co(II) and Ni(II) complexes containing the triazine unit: Supported by structural, spectral, and theoretical studies. *J. Coord. Chem.* **2018**, *71*, 3893–3911. [CrossRef]

34. Soliman, S.M.; Elsilk, S.E.; El-Faham, A. Syntheses, structure, Hirshfeld analysis and antimicrobial activity of four new Co (II) complexes with *s*-triazine-based pincer ligand. *Inorg. Chim. Acta* **2020**, *510*, 119753. [CrossRef]

35. Soliman, S.M.; Massoud, R.A.; Al-Rasheed, H.H.; El-Faham, A. Syntheses and Structural Investigations of Penta-Coordinated Co(II) Complexes with *Bis*-Pyrazolo-*s*-Triazine Pincer Ligands, and Evaluation of Their Antimicrobial and Antioxidant Activities. *Molecules* **2021**, *26*, 3633. [CrossRef]

36. Fathalla, E.M.; Abu-Youssef, M.A.M.; Sharaf, M.M.; El-Faham, A.; Barakat, A.; Badr, A.M.A.; Soliman, S.M.; Slawin, A.M.Z.; Woollins, J.D. Synthesis, Characterizations, Antitumor and Antimicrobial Evaluations of Novel Mn(II) and Cu(II) Complexes with NNN-tridentate *s*-Triazine-Schiff base Ligand. *Inorg. Chim. Acta* **2023**, *555*, 121586. [CrossRef]
37. Fathalla, E.M.; Abu-Youssef, M.A.M.; Sharaf, M.M.; El-Faham, A.; Barakat, A.; Haukka, M.; Soliman, S.M. Synthesis, X-ray Structure of Two Hexa-Coordinated Ni(II) Complexes with *s*-Triazine Hydrazine Schiff Base Ligand. *Inorganics* **2023**, *11*, 222. [CrossRef]
38. Fathalla, E.M.; Abu-Youssef, M.A.M.; Sharaf, M.M.; El-Faham, A.; Barakat, A.; Haukka, M.; Soliman, S.M. Supramolecular Structure and Antimicrobial Activity of Ni(II) Complexes with *s*-Triazine/Hydrazine Type Ligand. *Inorganics* **2023**, *11*, 253. [CrossRef]
39. Matsuno, T.; Karo, M.; Sasahara, H.; Watanabe, T.; Inaba, M.; Takahashi, M.; Yaguchi, S.I.; Yoshioka, K.; Sakato, M.; Kawashima, S. Synthesis and antitumor activity of benzimidazolyl-1,3,5-triazine and benzimidazolylpyrimidine derivatives. *Chem. Pharm. Bull.* **2000**, *48*, 1778–1781. [CrossRef]
40. Sherif, O.E.; Abdel-Kader, N.S. DFT calculations, spectroscopic studies, thermal analysis and biological activity of supramolecular Schiff base complexes. *Arab. J. Chem.* **2018**, *11*, 700–713. [CrossRef]
41. Rikagu Oxford Diffraction. *CrysAlisPro*; Rikagu Oxford Diffraction Inc.: Oxford, UK, 2020.
42. Sheldrick, G.M. Shelxt—Integrated space-group and crystal-structure determination. *Acta Crystallogr. Sect. C Struct. Chem.* **2015**, *A71*, 3–8. [CrossRef] [PubMed]
43. Sheldrick, G.M. Crystal structure refinement with SHELXL. *Acta Crystallogr. Sect. C Struct. Chem.* **2015**, *C71*, 3–8. [CrossRef]
44. Hübschle, C.B.; Sheldrick, G.M.; Dittrich, B. *ShelXle*: A Qt graphical user interface for *SHELXL*. *J. Appl. Crystallogr.* **2011**, *44*, 1281–1284. [CrossRef] [PubMed]
45. Spackman, M.A.; Jayatilaka, D. Hirshfeld Surface Analysis. *CrystEngComm* **2009**, *11*, 19–32. [CrossRef]
46. Lu, P.-L.; Liu, Y.-C.; Toh, H.-S.; Lee, Y.-L.; Liu, Y.-M.; Ho, C.-M.; Huang, C.-C.; Liu, C.-E.; Ko, W.-C.; Wang, J.-H. Epidemiology and antimicrobial susceptibility profiles of Gram-negative bacteria causing urinary tract infections in the Asia-Pacific region: 2009–2010 results from the Study for Monitoring Antimicrobial Resistance Trends (SMART). *Int. J. Antimicrob. Agents.* **2012**, *40*, S37–S43. [CrossRef]